Two-Stage Chance-Constrained Stochastic Thermal Unit Commitment for Optimal Provision of Virtual Inertia in Wind-Storage Systems

Tao Ding, *Senior Member, IEEE*, Ziyu Zeng, *Student Member, IEEE*, Ming Qu, *Student Member, IEEE*, João P. S. Catalão, *Senior Member, IEEE*, Mohammad Shahidehpour, *Fellow, IEEE*

***Abstract*—The frequency security problem becomes a critical concern in power systems when the system inertia is lowered due to the high penetration of renewable energy sources (RESs). A wind-storage system (WSS) controlled by power electronics can provide the virtual inertia to guarantee the fast frequency response after a disturbance. However, the provision of virtual inertia might be affected by the variability of wind power generation. To address this concern, we propose a two-stage chance-constrained stochastic optimization (TSCCSO) model to find the optimal thermal unit commitment (i.e., economic operation) and the optimal placement of virtual inertia (i.e., frequency stability) in a power grid using representative power system operation scenarios. An enhanced bilinear Benders decomposition method is employed with strong valid cuts to effectively solve the proposed optimization model. Numerical results on a practical power system show the effectiveness of the proposed model and solution method.**

***Index Terms*—Virtual inertia, bilinear Benders decomposition, chance-constrained stochastic programming, renewable energy.**

NOMENCLATURE

Indices and Sets

i	Index of units
k	Index of wind farms
t/j	Indices of discrete time periods
Q	Index of continuous time
s	Index of wind farm scenarios
b	Index of buses
m	Index of incentive demand response suppliers
L	Index of transmission lines
Ω_G	Set of units
Ω_W	Set of wind farms
Ω_B	Set of load buses

Parameters

T	Number of time periods
N_S	Set of scenarios
b_i, c_i	Generation cost coefficients of unit i
a_i, e_k	Reserve cost of unit i and wind farm k
SU_i/SD_i	Start-up/Shut-down cost of unit i
d_k	Virtual inertia cost of wind farm k
$x_{i,0}$	Initial status of unit i
$T_{i,0}$	Consecutive time of initial status of unit i
T_i^{on}	Minimum start-up time of unit i
T_i^{off}	Minimum shut-down time of unit i
Hw_k	Virtual inertia constant at wind farm k
Hg_i	Inertia constant of thermal unit i
D	Total effective system damping
$\Delta_{s,t}^{\max}$	Possible largest disturbance of power systems at time t in s-th scenario
$\Delta f_{nadir}^{\max}$	Maximum frequency increment at Nadir
$\Delta f_{QSS}^{\max}$	Maximum frequency increment at steady state
T_d	Delivery time of frequency response
t_{DB}	Dead-band time of governors
Δf_{DB}	Frequency increment at time t_{DB}
$RoCoF_{max}$	Maximum rate of change of frequency
M	A large number
$W_{k,s,t}^{f}$	s-th scenario of forecasted wind power at wind farm k at time t
$L_{b,s,t}$	s-th scenario for load at bus b at time t
$Rw_k^{\max}$	Reserve limit of wind farm k
$Rg_k^{\max}$	Reserve limit of unit i
π_s	Probability of the s-th scenario
$P_i^{\max}$	Maximum output of unit i
$P_i^{\min}$	Minimum output of unit i
Ru_i/Rd_i	Ramp up /ramp down rate of unit i
$F_l^{\max}$	Transmission line limit of line l
$G_{lk}/G_{li}/G_{lb}$	Distribution shift factor of line l to wind farm k, unit i and load bus b
λ_t	Confidence level for chance constraints at time t

Variables

$\Delta P_{i,t}/$ $\Delta W_{k,t}$	Generation increment of the i-th unit / k-th wind farm at time q after a disturbance
$\Delta f(q)$	Frequency increment at time q.
$W_{k,s,t}$	s-th scenario of wind generation at wind farm k at time t
$Rw_{k,s,t}$	Reserve of wind farm k at time t in s-th scenario
$Rg_{i,s,t}$	Reserve of unit i at time t in s-th scenario
$R_{s,t}$	Total regulating reserve at time t in s-th scenario
H	Total system inertia
$x_{i,t}$	Status of unit i at time t
$y_{k,t}$	Status of virtual inertia k at time t
$X_{i,t}$	Dummy variable for a bilinear term of unit i at time t
$Y_{k,s,t}$	Dummy variable for a bilinear term of wind farm k at time t in s-th scenarios
$\delta_{i,t}$	Start-up indicator of unit i at time t
$z_{i,t}$	Shut-down indicator of unit i at time t
$P_{i,t}$	Power generation of unit i at time t

This work was supported in part by National Natural Science Foundation of China (Grant 51977166), in part by China Postdoctoral Science Foundation (2017T100748), in part by Natural Science Foundation of Shaanxi Province (Grant 2020KW-022) and in part by Science and Technological Program of State Grid Shaanxi Electric Power Corporation (SGSN0000TKJS2001711).

Z. Zeng, T. Ding and M. Qu are with the Department of Electrical Engineering, Xi'an Jiaotong University, Xi'an, Shaanxi, 710049, China. (email: tding15@mail.xjtu.edu.cn)

J. P. S. Catalão is with the Faculty of Engineering of the University of Porto (FEUP) and INESC TEC, Porto, Portugal.

M. Shahidehpour is with the ECE Department, Illinois Institute of Technology, Chicago, IL 60616 USA.

I. Introduction

In order to solve the energy crisis and meet ecological sustainability requirements, many countries have taken various socioeconomic measures to promote the development of renewable energy sources (RESs) [1]-[3]. Traditional thermal units driven by fossil energy, are gradually replaced by wind turbines and photovoltaic (PV) units. The global PV and wind power installations in 2018 were 407 and 601 GW, respectively. The RES technology will continue to evolve progressively, changing the energy structure of the world [4]. However, RES development will have a significant impact on the thermal power system operation and security since any replacement of conventional thermal generation units by RESs will reduce the power system inertia which refers to the kinetic energy stored in rotating synchronous machines [5].

RES units placed in a power grid are equipped with power electronic converters. For instance, wind unit converters decouple the units from the main grid and thus the wind generator rotational speed will be independent of the system frequency. In contrast, the inherent rotational inertia of synchronous machines and the damping provided by governors contribute to the system stability when a power grid contingency occurs. Accordingly, large-scale RES integrations could weaken the power grid ability to resist large frequency changes in response to disturbances, raising concerns about the system frequency stability [6].

As inertial sources in a power grid are complex and diverse, several studies have quantified the available inertia by either measurement or analytic methods. A process was developed in [7] to measure transient frequency by generator outage tests for estimating the available inertia and on-line spinning-reserve requirements. Tracing electromechanical wave propagation at the power distribution level, [8] established a non-invasive way to measure changes in inertia with high penetration of RESs. In addition to experimental methods, a statistics-based model using historical data was proposed in [9] to estimate the real-time system inertia under observed steady-state conditions with relatively small frequency changes.

Reference [10] investigated the system response to small disturbances applied to a linear model of synchronous machines, pointing out that the inertia of conventional generation units with an impact on power system stability depended on their sizes, speeds, and types. In [11], the load-side inertia was estimated by a white-box method to track the system frequency in disturbances. In particular, the impacts of sampling rates were investigated. The results showed that the load inertia time constant was less than 1 second in most cases. Besides, an analytic model was set up in [12] to assess the total system inertia response, using the kinetic energy stored in rotating wind turbines Note that there would be optimal inertia constant for each system which will maintain the balance between economy and operational security.

To address the frequency stability problem for a low-inertia power system, it is essential to incorporate frequency-dependent constraints in economic dispatch (ED) and unit commitment (UC) models. It was reported in [13] that the potential shortfalls of the system inertia were affected by the non-synchronous RESs and then a strategic UC model was set up to mitigate frequency instability risks. In [14], a general expression of inertial response requirements was derived by keeping the system within a given frequency range, and the corresponding dynamic system model was established by using second-order differential equations. Mixed-integer linear programming for the day-ahead UC model was proposed in [15], which simultaneously considered both primary reserve constraints and frequency regulation constraints. The results indicated that the coordination of UC and frequency regulation could reduce the frequency fluctuation during disturbances.

Regarding the system inertia as an economic index of power system operations, [16] provided a UC model with fast-charging storage equipment, which was solved by a nonlinear-constraint approximation method. The concept of frequency security margin, defined as the maximum power imbalance that the system can tolerate, was proposed in [17], and a frequency constrained UC incorporating the frequency security margin was proposed to evaluate the impact of renewable energy on power system security. Such a frequency constrained UC method can help power system dispatchers make more secure power generation plans. Nonlinear frequency constraints were derived by performing several dynamic simulations in [18] to ensure that the rate of change of frequency (RoCoF) and frequency deviations are within security thresholds. Besides, a frequency-constrained stochastic ED model was utilized in [19] to incorporate wind uncertainty and frequency constraints. Reference [20] proposed a stochastic UC model that considered not only wind energy forecast errors but also generation outage uncertainties. The model optimized system operations by coordinating energy production, operating reserves, and inertia-dependent fast frequency responses.

The more recent developments in power electronics introduce additional opportunities for installing new devices and controllers to provide virtual inertia to power systems, which perform like synchronous generators to flexibly adjust the active power in response to frequency variations [21]-[24]. It was reported in [25] that the kinetic energy of wind turbines and energy storage can deliver necessary virtual inertia responses by power electronic converters, while PV units could not provide respective inertia responses because of the lack of rotating energy. This paper provided a theoretical basis for the provision of virtual inertia by the wind-storage system (WSS) controlled by power electronics. Reference [26] suggested that the inertia of a power-electronic-controlled wind turbine depended on the turbine type, size, and installed gearbox. Fast-acting storage was designed in [27] by immediately injecting additional power to cope with the generator outage, so that the dynamic performance of the system frequency can be improved.

Some of the power system optimization models consider virtual inertia. In [28], the virtual inertia of wind farms and solar PV power stations was simulated and the location of virtual inertia in the power grid optimized by a genetic algorithm. The proposed method could optimize the virtual inertia location efficiently and improve the frequency stability of the power system. In [29], the system virtual inertia constants were optimally selected to maintain the frequency stability with the lowest cost via a multi-objective optimization model including inertia constants, frequency droop coefficients, and load frequency controller parameters. The proposed method could increase the microgrid inertia at a low cost to maintain frequency stability. Reference [30] suggested that the

placement of virtual inertia in the power grid might affect the frequency stability and thus an optimal inertia placement model was established.

The previous papers have achieved good results for enhancing the frequency stability of low-inertia power systems by utilizing virtual inertia devices. Placing the virtual inertia in power systems can enhance their frequency stability but may also increase the system operational cost. However, few papers have studied the coordination of the day-ahead UC and the optimal placement of virtual inertia. Hence, the main contributions of this paper are summarized as follows:

(i) For power-electronic driven power systems, the impact of the virtual inertia of WSS is modeled in the daily UC scheduling. The available power system inertia is quantified considering the existing thermal generating units and WSS to guarantee the frequency security when a disturbance occurs. Then, a two-stage chance-constrained stochastic optimization (TSCCSO) model is set up to analyze the impact of RES uncertainties on devising a trade-off between frequency security and economic operation in power systems.

(ii) In order to reduce the computational burden on a large-scale stochastic optimization model with a significant number of scenarios, an enhanced bilinear Benders decomposition is designed to solve the large TSCCSO problem, where strong valid cuts are generated to improve the convergence performance.

The rest of the paper is organized as follows. Section II quantifies the frequency performance by three metrics that analyze the impact of power system inertia on the frequency performance. Then, a two-stage chance-constrained stochastic UC model is set up and a bilinear Benders decomposition with strong valid cuts is designed in Section III. In Section IV, numerical results on the practical test systems demonstrate the effectiveness of the proposed model. Finally, Section V summarizes conclusions.

II. Quantifying Impacts of System Inertia on Frequency

When the system suffers a disturbance, the system frequency will be changed accordingly due to the imbalance between the power generation and load demand. Since the secondary frequency drop is very fast (usually in seconds), while the time scale of UC and economic dispatch is usually within minutes to hours. Thus, the fast dynamic component of the secondary frequency control is not considered while the primary frequency (usually seconds to minutes) is kept [19],[30]. Fig. 1 depicts the transient frequency for different system inertia, where three metrics are used to quantify the frequency including: 1) RoCoF; 2) frequency at Nadir; 3) Quasi-Steady-State (QSS) frequency. If the system has insufficient inertia, the slope of frequency deviation, maximum frequency increment, and QSS frequency increment will become larger. The practical regulations provided by the State Grid of China pointed out that RoCoF, Nadir, and QSS frequency should be limited to guarantee the system reliability and resilience in extreme conditions. Specifically, RoCoF should be no larger than 0.125 Hz/s, Nadir should be higher than 49.2 Hz, and the final QSS frequency should not be lower than 49.8 Hz within the first 60 seconds.

Fig. 2 presents the schematic diagram of the virtual inertia provided by the WSS. Specifically, the upper half of Fig. 2 is the power system with wind farms, and the lower half is the topology diagram of a certain wind farm with WSS controlled by power electronics. Here, we consider that WSS controlled by power electronics can immediately provide the extra power to react to any frequency changes. From the power system perspective, the WSS reaction which is in response to a disturbance contributes to the virtual inertia of power systems. This leads WSS to act as a virtual power plant, which is analogous to a thermal unit [30]-[32]. Since there are many operation scenarios, the frequency security should be analyzed for each scenario. Let the virtual inertia provided by wind farm k be Hw_k.

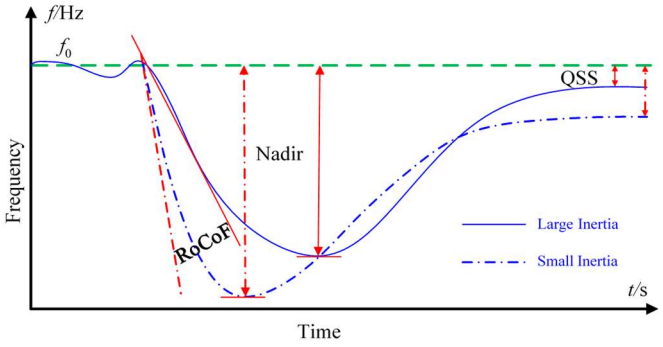

Fig. 1. Quantifying transient frequency for different system inertia

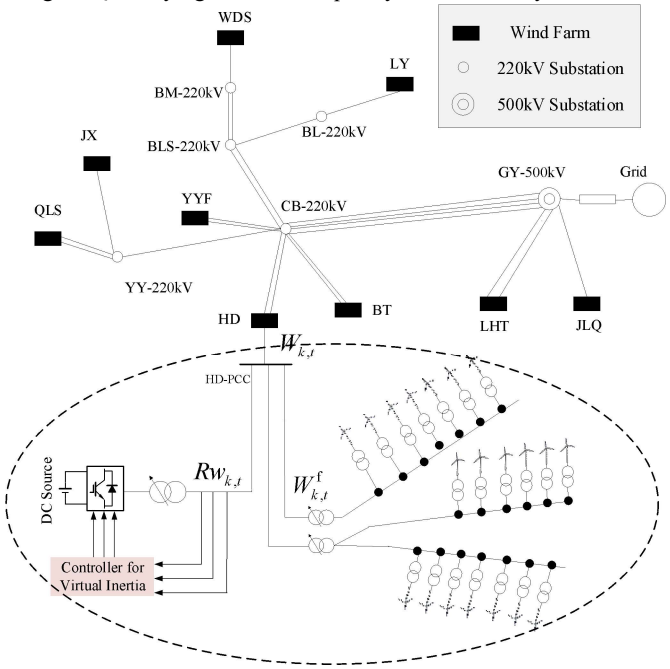

Fig. 2 WSS for the provision of virtual inertia [33]

The total system inertia H can be expressed as (1). Meanwhile, the wind farm in the scenario s at time t should have reserve energy $Rw_{k,s,t}$ at each time period to provide the potential frequency response. If WSS is used to provide virtual inertia, the wind unit output would be the forecasted output minus the reserve; otherwise, the wind power output is equal to its forecasted value.

$$H_t = \sum_{k\in\Omega_W} Hw_k y_{k,t} + \sum_{i\in\Omega_G} Hg_i x_{i,t} \tag{1a}$$

$$W_{k,s,t} = W^{\mathrm{f}}_{k,s,t} - Rw_{k,s,t},\ 0 \le Rw_{k,s,t} \le Rw^{\max}_k y_{k,t},\ \forall k, \forall t, \forall s \tag{1b}$$

This article has been accepted for publication in a future issue of this journal, but has not been fully edited. Content may change prior to final publication. Citation information: DOI 10.1109/TPWRS.2021.3051523, IEEE Transactions on Power Systems

A first-order ordinary differential equation (ODE) is employed to quantify the three metrics for frequency changes as

$$2H_t\frac{\partial\Delta f(q)}{\partial q}+D_t*\Delta f(q)=\sum_{i\in\Omega_g}\Delta P_{i,s,t}+\sum_{k\in\Omega_w}\Delta W_{k,s,t}+\Delta_{s,t}^{\max} \quad (2)$$

In [20], it was reported that $\Delta P_{i,t}(q)$ and $\Delta W_{k,t}(q)$ are piecewise linear functions as

$$\Delta P_{i,s}(q)=\begin{cases}0 & if \quad q\le t_{DB}\\ Rg_{i,s,t}(q-t_{DB})/T_d & if \quad t_{DB}\le q\le t_{DB}+T_d\\ Rg_{i,s,t} & q\ge t_{DB}+T_d\end{cases} \quad (3a)$$

$$\Delta W_{k,s}(q)=\begin{cases}0 & if \quad q\le t_{DB}\\ Rw_{k,s,t}(q-t_{DB})/T_d & if \quad t_{DB}\le q\le t_{DB}+T_d\\ Rw_{k,s,t} & q\ge t_{DB}+T_d\end{cases} \quad (3b)$$

Here, (3a) and (3b) indicate that when the time is shorter than the dead band, the increments of generators and WSSs are zero; otherwise, governor responses are linear functions with a fixed slope until the response reaches its um limit.

The ODE (2) with the governor response of units and wind farms (3) is solved and the closed-form solution of the frequency increment is expressed as

$$\Delta f(q)=\begin{cases}\dfrac{\Delta_{s,t}^{\max}}{D_t}\left(1-e^{-\frac{D_t}{2H_t}q}\right) & q\le t_{DB}\\ \dfrac{T_dD_t\Delta_{s,t}^{\max}+2R_{s,t}H_t-R_tD_t(q-t_{DB})}{T_dD^2}- & \\ \dfrac{T_dD_t\Delta_{s,t}^{\max}-T_dD_t^2\Delta f(t_{DB})+2R_{s,t}H_t}{T_dD^2}e^{-\frac{D_t}{2H_t}(q-t_{DB})} & T_d+t_{DB}\ge q\ge t_{DB}\\ \dfrac{\Delta_{s,t}^{\max}-R_t}{D_t}-\left(\dfrac{\Delta_{s,t}^{\max}-R_{s,t}}{D_t}-\Delta f(T_d+t_{DB})\right)e^{-\frac{D_t}{2H_t}(q-T_d-t_{DB})} & q\ge T_d+t_{DB}\end{cases}$$
$$,\forall t,\forall s \quad (4)$$

where $R_{s,t}=\sum_{i\in\Omega_G}Rg_{i,s,t}+\sum_{k\in\Omega_W}Rw_{k,s,t}$ is the total regulating reserve of the *s*-th scenario at time *t*. According to (4), the maximum RoCoF occurs first after the disturbance. Given the requirement of the maximum RoCoF, the total system inertia should satisfy the following equation,

$$H_t=\sum_{k\in\Omega_W}Hw_k y_{k,t}+\sum_{i\in\Omega_G}Hg_i x_{i,t}\ge\frac{\Delta_{s,t}^{\max}}{2RoCoF_{\max}} \quad (5)$$

The frequency at Nadir is the minimum frequency, which is calculated by $\partial\left|\Delta f(q)\right|/\partial q=0$, giving

$$H_tR_{s,t}=\left(\sum_{k\in\Omega_W}H_{w,k}y_{k,t}+\sum_{i\in\Omega_G}H_{g,t}x_{i,t}\right)\left(\sum_{i\in\Omega_G}Rg_{i,s,t}+\sum_{k\in\Omega_W}Rw_{k,s,t}\right)\ge\kappa_t$$
$$,\forall t,\forall s \quad (6)$$

where $\kappa_{s,t}$ can be obtained by the solution of

$$\frac{2\kappa_{s,t}}{T_d}\log\left(\frac{2\kappa_{s,t}}{2\kappa_t+T_dD_t\left(\Delta_{s,t}^{\max}-D_t\Delta f_{DB}\right)}\right)=D_t^2\left(\Delta f_{nadir}^{\max}-\Delta f_{DB}\right)-D_t\left(\Delta_{s,t}^{\max}-D_t\Delta f_{DB}\right) \quad ,\forall t,\forall s \quad (7)$$

The QSS frequency can be derived by allowing $t\to+\infty$ in (4), which gives

$$\frac{\Delta_t^{\max}-\left(\sum_{i\in\Omega_G}Rg_{i,s,t}+\sum_{k\in\Omega_W}Rw_{k,s,t}\right)}{D_t}\le\Delta f_{QSS}^{\max} \quad ,\forall t,\forall s \quad (8)$$

Finally, (5), (6), (8), and (9) can quantify the power system frequency performance with respect to inertia. Here, (5), (8), and (9) are all linear inequalities, while (6) is a bilinear constraint. Note that the bilinear term in (6) consists of continuous and binary variables, which are exactly linearized by

$$\begin{aligned}&\mathrm{P}\left(\sum_{k\in\Omega_W}Hw_kY_{k,s,t}+\sum_{i\in\Omega_G}Hg_iX_{i,t}\ge\kappa_{s,t}\right)\ge1-\lambda_t\\ &-M(1-x_{i,t})\le X_{i,s,t}-\sum_{i\in\Omega_G}Rg_{i,s,t}-\sum_{k\in\Omega_W}Rw_{k,s,t}\le M(1-x_{i,t})\\ &-M(1-y_{k,t})\le Y_{k,s,t}-\sum_{i\in\Omega_G}Rg_{i,s,t}-\sum_{k\in\Omega_W}Rw_{k,s,t}\le M(1-y_{k,t})\\ &-Mx_{i,t}\le X_{i,s,t}\le Mx_{i,t},\ -My_{k,t}\le Y_{k,s,t}\le My_{k,t}\end{aligned}$$
$$,\forall i,\forall k,\forall t,\forall s \quad (9)$$

III. Two-Stage Chance-Constrained Stochastic UC Model Considering Optimal Virtual Inertia

The wind power generation forecast error is usually stochastic which may affect the power system operation and the provision of the power system virtual inertia. In order to address the uncertainty, scenario analyses are deployed to select representative scenarios from the probability distribution of the wind power generation forecast error. The scenario value and the corresponding probability are $\left(W_{k,s,t}^{\mathrm{f}},\pi_s\right)$. To balance the system security and economy, a two-stage chance-constrained stochastic program (TSCCSO) is set up. At the first stage, a UC is formulated to immune the solution against all representative scenarios for the optimal provision of virtual inertia. At the second stage, given the first-stage decisions, the ED solution is calculated for each scenario. The detailed optimization model is written as follows [34],[35].

A. Objective Function

$$\min \quad C_{\mathrm{main}}=\left(C_{\mathrm{oper}}+C_{\mathrm{resev}}+C_{\mathrm{virt}}\right) \quad (10a)$$

where C_{oper} is the total operation cost of the power system; C_{resev} represents the reserve cost for thermal and W generation units, and C_{virt} is the cost of virtual inertia provision. Specifically, we have

$$C_{\mathrm{oper}}=\sum_{s=1}^{N_S}\pi_s\sum_{t=1}^{T}\sum_{i\in\Omega_G}\left(b_iP_{i,s,t}+c_ix_{i,t}+SU_i\delta_{i,t}+SD_iz_{i,t}\right) \quad (10b)$$

$$C_{\mathrm{resev}}=\sum_{s=1}^{N_S}\pi_s\sum_{t=1}^{T}\left(\sum_{i\in\Omega_G}a_iRg_{i,t,s}+\sum_{k\in\Omega_W}e_kRw_{k,t,s}\right) \quad (10c)$$

$$C_{\mathrm{virt}}=\sum_{t=1}^{T}\sum_{k\in\Omega_W}d_ky_{k,t} \quad (10d)$$

B. First Stage Constraints

The first stage constraints include

$$x_{i,t}-x_{i,t-1}=\delta_{i,t}-z_{i,t},\forall i\in\Omega_{\mathrm{G}},\forall t \quad (11)$$

$$\sum_{j=\max(t-T_i^{on}+1,1)}^{t} \delta_{i,j} \le x_{i,t} \quad ,\forall i \in \Omega_G, \quad \forall t \in \left[\max\left\{0, \min\left[T, x_{i,0}\left(T_i^{on}-T_{i,0}\right)\right]\right\}+1, T \right] \tag{12}$$

$$\sum_{j=\max(t-T_i^{off}+1,1)}^{t} z_{i,j} \le x_{i,t} \quad ,\forall i \in \Omega_G, \quad \forall t \in \left[\max\left\{0, \min\left[T, \left(1-x_{i,0}\right)\left(T_i^{off}-T_{i,0}\right)\right]\right\}+1, T \right] \tag{13}$$

where (11) presents the relationship among start-up and shut-down indicator and unit status; (12) and (13) characterizes minimum start-up and shut-down times of units;

C. Second Stage Constraints

The second stage constraints include

$$\begin{aligned} &P_{i,s,t}-P_{i,s,t-1} \le x_{i,t-1}Ru_i+\left(1-u_{i,t-1}\right)P_i^{\max} \\ &P_{i,s,t-1}-P_{i,s,t} \le x_{i,t}Rd_i+\left(1-u_{i,t}\right)P_i^{\min} \\ &x_{i,t}P_i^{\min} \le P_{i,s,t} \le x_{i,t}P_i^{\max}-Rg_{i,s,t} \\ &0 \le Rg_{i,s,t} \le Rg_i^{\max}x_{i,t} \end{aligned} \quad ,\forall i \in \Omega_G, \forall t, \forall s \tag{14}$$

$$\sum_{i\in\Omega_G} P_{i,s,t}+\sum_{k\in\Omega_W} W_{k,s,t}=\sum_{b\in\Omega_B} L_{b,t} \quad ,\forall t, \forall s \tag{15}$$

$$-F_l^{\max} \le \sum_{k\in\Omega_W} G_{lk}W_{k,s,t}+\sum_{i\in\Omega_G} G_{li}P_{i,s,t}-\sum_{b\in\Omega_B} G_{lb}L_{b,t} \le F_l^{\max} \quad ,\forall l, \forall t, \forall s \tag{16}$$

$$\begin{aligned} &W_{k,s,t}=W_{k,s,t}^{\mathrm{f}}-Rw_{k,s,t} \\ &0 \le Rw_{k,s,t} \le Rw_{k,t}^{\max}y_{k,t} \end{aligned} \quad ,\forall k, \forall t, \forall s \tag{17}$$

$$H=\sum_{k\in\Omega_W} Hw_kW_k^{\max}y_{k,t}+\sum_{i\in\Omega_G} Hg_iP_i^{\max}x_{i,t} \tag{18}$$

$$\mathrm{P}\left(H \ge \frac{\Delta_{s,t}^{\max}}{2RoCoF_{\max}} \right), \forall t \tag{19}$$

$$\mathrm{P}\left(\sum_{i\in\Omega_G} Rg_{i,s,t}+\sum_{k\in\Omega_W} Rw_{k,s,t} \ge \Delta_{s,t}^{\max}-D\Delta f_{QSS}^{\max} \right) \ge 1-\lambda_t \quad ,\forall s, \forall t \tag{20}$$

$$\begin{aligned} &\mathrm{P}\left(\sum_{k\in\Omega_W} Hw_kY_{k,s,t}+\sum_{i\in\Omega_G} Hg_iX_{i,t} \ge \kappa_{s,t} \right) \ge 1-\lambda_t \\ &-M\left(1-x_{i,t}\right) \le X_{i,s,t}-\sum_{i\in\Omega_G} Rg_{i,s,t}-\sum_{k\in\Omega_W} Rw_{k,s,t} \le M\left(1-x_{i,t}\right) \\ &-M\left(1-y_{k,t}\right) \le Y_{k,s,t}-\sum_{i\in\Omega_G} Rg_{i,s,t}-\sum_{k\in\Omega_W} Rw_{k,s,t} \le M\left(1-y_{k,t}\right) \\ &-Mx_{i,t} \le X_{i,s,t} \le Mx_{i,t}, -My_{k,t} \le Y_{k,s,t} \le My_{k,t} \end{aligned} \quad ,\forall i, \forall k, \forall t, \forall s \tag{21}$$

where (14) describes the limits on ramp rate, reserve, and generation output for each unit; (15) is the power balance constraint; (16) ensures the power flow on each transmission line is limited to its allowable range; (17) is the reserve constraint in a wind farm. If a wind farm provides the virtual inertia, the reserve should be considered; (18) quantifies the total power system inertia, and (19)-(21) are the chance constraints to trade off the power system economy with frequency stability.

D. Solution Method

The above TSCCSO is stated as

$$\min \quad \boldsymbol{c}^T\boldsymbol{x}+\boldsymbol{d}^T\boldsymbol{y}(\xi) \tag{22a}$$

$$s.t. \quad \boldsymbol{A}\boldsymbol{x} \ge \boldsymbol{b} \tag{22b}$$

$$\mathrm{P}\left\{\boldsymbol{G}\boldsymbol{x}+\boldsymbol{H}\boldsymbol{y}(\xi) \ge \boldsymbol{h}(\xi)\right\} \ge 1-\lambda \tag{22b}$$

$$\boldsymbol{x} \in \mathrm{Z}\times\mathrm{R} \ , \ \boldsymbol{y}(\xi) \in \mathrm{R} \tag{22b}$$

where $\boldsymbol{x}$ are first-stage decision variables; $\boldsymbol{y}(\xi)$ are second-stage decision variables associated with scenarios; λ is the risk-averse level; $\boldsymbol{h}(\xi)$ is the random vector depending on scenarios; $\boldsymbol{G}$, $\boldsymbol{H}$, $\boldsymbol{A}$, and $\boldsymbol{b}$ are deterministic matrices and vector; $\boldsymbol{c}$ and $\boldsymbol{d}$ are coefficient vectors of first- and second-stage variables.

The chance constraints are explicitly written, using the N_s scenarios, as a series of linear constraints by a bilinear formulation, where

$$\min \quad \boldsymbol{c}^T\boldsymbol{x}+\sum\nolimits_{s=1}^{N_s} \pi_s\boldsymbol{d}^T\boldsymbol{y}_s\left(1-z_s\right) \tag{23a}$$

$$s.t. \quad \boldsymbol{A}\boldsymbol{x} \ge \boldsymbol{b} \tag{23b}$$

$$\left(\boldsymbol{G}\boldsymbol{x}+\boldsymbol{H}\boldsymbol{y}_s-\boldsymbol{h}_s\right)\left(1-z_s\right) \ge 0, \quad s=1,\ldots,N_s \tag{23c}$$

$$\sum\nolimits_{s=1}^{N_s} \pi_s z_s \le \lambda \tag{23d}$$

$$\boldsymbol{x} \in \mathrm{Z}\times\mathrm{R} \ , \ \boldsymbol{y}_s \in \mathrm{R} \ , \ z_s \in \{0,1\}, s=1,\ldots,N_s \tag{24e}$$

where z_s is a binary variable for choosing the enforced constraint. The model suggests that when z_s=0, $\boldsymbol{G}_s\boldsymbol{x}+\boldsymbol{H}_s\boldsymbol{y}_s \ge \boldsymbol{h}_s$ must be satisfied and the corresponding resource will be considered; when z_s=1, $\boldsymbol{G}_s\boldsymbol{x}+\boldsymbol{H}_s\boldsymbol{y}_s \ge \boldsymbol{h}_s$ does not need to be satisfied and the recourse in the objective function is zero.

Given any first-stage $\boldsymbol{x}^v$, the model is only related to $\boldsymbol{y}_s$ and z_s. Furthermore, we derive the dual model, in which z_s has two possible values, either 1 or 0. If z_s=1, the decision variables will disappear, leading the model irrelevant; If z_s=0, the optimization model becomes (24) with $\boldsymbol{y}_s$ as the decision variables in which the constant value $\boldsymbol{c}^T\boldsymbol{x}^v$ can be ignored. Hence,

$$\min \quad \sum\nolimits_{s=1}^{N_s} \pi_s\boldsymbol{d}^T\boldsymbol{y}_s \tag{24a}$$

$$s.t. \quad \boldsymbol{H}\boldsymbol{y}_s \ge \boldsymbol{h}_s-\boldsymbol{G}\boldsymbol{x}^v, \quad s=1,\ldots,N_s \tag{24b}$$

$$\boldsymbol{y}_s \in \mathrm{R} \ , s=1,\ldots,N_s \tag{24c}$$

The dual optimization model of the linear model (24) is obtained in (25), which is separable in the N_s scenarios. Thus, for the s-th scenario, we have the dual model as

$$\max \quad \left(\boldsymbol{h}_s-\boldsymbol{G}\boldsymbol{x}^v\right)^T\boldsymbol{u}_s \tag{25a}$$

$$s.t. \quad \boldsymbol{H}^T\boldsymbol{u}_s \le \boldsymbol{d} \tag{25b}$$

$$\boldsymbol{u}_s \ge 0, \ \boldsymbol{u}_s \in \mathrm{R} \tag{25c}$$

Denote the sets of extreme points and rays as $\Theta^s=\left\{u_s^1,\ldots,u_s^v,\ldots,u_s^{|\Theta^s|}\right\}$ and $\Pi^s=\left\{o_s^1,\ldots,o_s^v,\ldots,o_s^{|\Pi^s|}\right\}$, where $|\bullet|$ denotes the cardinality of a set. According to the duality theory, if (25) is feasible, the optimal solution must arrive at an extreme point. Then, the bilinear Benders decomposition is designed as

$$\min \quad \boldsymbol{c}^T\boldsymbol{x}+\sum\nolimits_{s=1}^{N_s} \pi_s\boldsymbol{Q}_s \tag{26a}$$

$$s.t. \quad \boldsymbol{A}\boldsymbol{x} \ge \boldsymbol{b} \tag{26b}$$

$$\left(\boldsymbol{h}_s-\boldsymbol{G}\boldsymbol{x}\right)^T\boldsymbol{u}_s^v\left(1-z_s\right)\le\boldsymbol{Q}_s,\ \ v\in\Theta^s,\ s=1,\ldots,N_s \tag{26c}$$

$$\left(\boldsymbol{h}_s-\boldsymbol{G}\boldsymbol{x}\right)^T\boldsymbol{o}_s^v\left(1-z_s\right)\le 0,\ \ v\in\Pi^s,\ s=1,\ldots,N_s \tag{26d}$$

$$\sum\nolimits_{s=1}^{N_s}\pi_s z_s\le\lambda \tag{26e}$$

$$\boldsymbol{x}\in \mathrm{Z}\times\mathrm{R},\ \ \boldsymbol{y}_s\in\mathrm{R},\ \ z_s\in\{0,1\},\ s=1,\ldots,N_s \tag{26f}$$

where if (25) is feasible, the optimality cut (26c) is added; otherwise, the feasibility cut (26d) is added. It should be noted that the bilinear terms in (26c) and (26d) can be exactly linearized by the McCormick reformulation as

$$\begin{aligned}&\left(\boldsymbol{h}_s-\boldsymbol{G}\boldsymbol{p}\right)^T\boldsymbol{u}_s^v\le\boldsymbol{Q}_s\\&-M\left(1-z_s\right)\le\boldsymbol{p}\le M\left(1-z_s\right),\ \ v\in\Theta^s,\ s=1,\ldots,N_s\\&-Mz_s\le\boldsymbol{p}-\boldsymbol{x}\le Mz_s\end{aligned} \tag{27a}$$

$$\begin{aligned}&\left(\boldsymbol{h}_s-\boldsymbol{G}\boldsymbol{q}\right)^T\boldsymbol{o}_s^v\le 0\\&-M\left(1-z_s\right)\le\boldsymbol{q}\le M\left(1-z_s\right),\ \ v\in\Pi^s,\ s=1,\ldots,N_s\\&-Mz_s\le\boldsymbol{q}-\boldsymbol{x}\le Mz_s\end{aligned} \tag{27b}$$

Furthermore, we will design a strong valid cut to enhance the convergence of the bilinear Benders decomposition. At first, the Jensen's inequality for (23) is given as

Theorem 1 [36]: Let z_s^v and x^v be the optimal values during the v-th iteration. The optimal expected recourse will satisfy the following inequalities,

$$\begin{aligned}&\sum\nolimits_{s=1}^{N_s}\pi_s\boldsymbol{d}^T\boldsymbol{y}_s\left(1-z_s^v\right)\ge\min\ \left(1-\sum\nolimits_{s=1}^{N_s}\pi_s z_s\right)\boldsymbol{d}^T\bar{\boldsymbol{y}}\\&s.t.\ \ \left(1-\sum\nolimits_{s=1}^{N_s}\pi_s z_s\right)\boldsymbol{H}\bar{\boldsymbol{y}}\ge\sum\nolimits_{s=1}^{N_s}\pi_s\left(1-z_s\right)\left(\boldsymbol{h}_s-\boldsymbol{G}\boldsymbol{x}^v\right),\\&\sum\nolimits_{s=1}^{N_s}\pi_s z_s\le\lambda,\quad\bar{\boldsymbol{y}}\ge 0,\quad z_s=\{0,1\}\end{aligned} \tag{28}$$

where $\bar{\boldsymbol{y}}$ is a newly introduced variable.

Theorem 1 suggests that the first constraint in (28) will provide a strong valid cut by replacing $\boldsymbol{x}^v$ with $\boldsymbol{x}$, such that

$$\sum\nolimits_{s=1}^{N_s}\pi_s\boldsymbol{Q}_s\left(1-z_s^v\right)\ge\left(1-\sum\nolimits_{s=1}^{N_s}\pi_s z_s\right)\boldsymbol{d}^T\bar{\boldsymbol{y}},\quad\bar{\boldsymbol{y}}\ge 0 \tag{29a}$$

$$\left(1-\sum\nolimits_{s=1}^{N_s}\pi_s z_s\right)\boldsymbol{H}\bar{\boldsymbol{y}}\ge\sum\nolimits_{s=1}^{N_s}\pi_s\left(1-z_s\right)\left(\boldsymbol{h}_s-\boldsymbol{G}\boldsymbol{x}\right) \tag{29b}$$

Moreover, we define an integer K such that $K/N_s\le\lambda\le\left(K+1\right)/N_s$ and $\pi_s=1/N_s$. Then, we arrive at $\sum\nolimits_{s=1}^{N_s}z_s=K$ and (29) can be further simplified as

$$\sum\nolimits_{s=1}^{N_s}\pi_s\boldsymbol{Q}_s\left(1-z_s^v\right)\ge\frac{K}{N_s-K}\boldsymbol{d}^T\bar{\boldsymbol{y}},\quad\bar{\boldsymbol{y}}\ge 0 \tag{30a}$$

$$\boldsymbol{H}\bar{\boldsymbol{y}}\ge\sum\nolimits_{s=1}^{N_s}\frac{1-z_s}{N_s-K}\boldsymbol{h}_s-\boldsymbol{G}\boldsymbol{x}, \tag{30b}$$

Finally, the flowchart of the bilinear Benders decomposition is presented in Table I. At the beginning, we neglect the Benders cuts (26c)-(26d) and the strong valid cut (30). Solving (26) gives the initial estimate of the optimal solution (x^0, z_s^0). Then, we fix the first-stage variable x^0 and solve the second-stage subproblems (25) which are scenario-independent and can be handled in parallel. We solve (25) only for the scenario with z_s^0=0. Furthermore, we derive the traditional Benders cuts by (26c)-(26d) and strong valid cuts by (30), which are all added into (26) to improve the lower bound.

Table I Flowchart of the enhanced bilinear Benders decomposition

Algorithm: Bilinear Benders Decomposition	
Input	Given the parameters of the model (23)
Output	Optimal solution and optimal value
Step 1	Set LB=−∞, UB=+∞, v←0, Θ^s←Ø and Π^s←Ø
Step 2	Solve the master problem (26) with the linearized constraints (27) and strong valid cuts (30)
Step 3	If the model is infeasible, stop; otherwise, obtain the optimal value Z^v and optimal solution (x^v, z_s^v)
Step 4	Update the lower bound by LB=Z^v
Step 5	For each scenario s, choose z_s^v=0 and do
Step 6	Solve the model (25). If the model is bounded, obtain the optimal solution $\boldsymbol{u}_s^v$ and optimal value Q_s, otherwise, obtain the extreme ray $\boldsymbol{o}_s^v$.
Step 7	Update the two sets by $\Theta^s=\Theta^s\cup\{\boldsymbol{u}_s^v\}$ and $\Pi^s=\Pi^s\cup\{\boldsymbol{o}_s^v\}$.
Step 8	Add a strong valid cut (30) into (26)
Step 9	Update the upper bound by UB=min{UB, $\boldsymbol{c}^T\boldsymbol{x}^v+\sum\nolimits_{s=1}^{N_s}\pi_s\boldsymbol{Q}_s\left(1-z_s^v\right)$}
Step 10	If $\left(UB-LB\right)/LB\le\varepsilon$, stop with the optimal solution (x^v, z_s^v) and optimal value UB. For each z_s^v=0, solving (24) gives the optimal solution $\boldsymbol{y}_s^v$; otherwise, v←v+1 and goto **Step 2**

IV. Case Studies

The proposed model is verified on a practical power system in China shown in Fig. 3, which includes 197 buses, 43 thermal units, 27 wind farms , and 232 transmission lines. The system parameters are given as follows: T_d=10s; D=0.1 p.u.; Hw_k=6s [37]; Hg_i=6s [38]; ramp up/down is 25% of the total generation capacity. The Latin hypercube sampling method is applied to the historical wind speed data for a wind farm in China to generate the representable stochastic wind speed scenarios with the corresponding probabilities for the stochastic programming model [39]-[40]. The data are available in [41]. Fig. 4. gives the forecasted values of load and wind power generation with 100 scenarios, where peak load periods are 8:00-12:00 and 18:00-22:00, the valley load periods are 2:00-6:00, the peak wind power periods are 1:00-5:00, and the valley wind power periods are 12:00-20:00. Moreover, to simulate the stochastic nature of wind power, 10 scenarios are selected and the computation tasks are carried out using GUROBI 8.0 on a laptop with Inter Core 7 CPU (3.60GHz).

At first, with and without considering virtual inertia are compared in Table II, where $\Delta_t^{\max}$ equals to a quarter of the total wind farm output. In the latter case, all three frequency metrics will be violated, while the frequency metrics will be strictly satisfied for λ=1. When λ is smaller than 1, chance constraints will be activated and the three frequency metrics will be increased by lowering λ. This suggests that the frequency will decay more rapidly. In contrast, the three costs are also compared in Table II, where all costs are larger. This is because considering frequency security constraints will require a higher system inertia. Accordingly, thermal units with large inertia may be deployed, while virtual inertia provided by WSS will also be needed. Overall, the simulation results indicate the tradeoff between cost and frequency security as we alter λ.

This article has been accepted for publication in a future issue of this journal, but has not been fully edited. Content may change prior to final publication. Citation information: DOI 10.1109/TPWRS.2021.3051523, IEEE Transactions on Power Systems

Table III compares three frequency metrics and costs for three different virtual inertia constants (i.e., Hw_k=4s, Hw_k=6s, Hw_k=8s). Larger virtual inertia constant indicates that the system inertia will be increased for the same status of virtual inertia. Thus, as the virtual inertia constant increases, the operation cost, including those of UC and dispatch, is lower while the virtual inertia provision cost becomes higher. Overall, the total cost will be reduced. On the other hand, for λ=0.95, the frequency metrics will be violated, but the larger virtual inertia constant does not make the frequency metrics worse. RoCoF and Δf_{Nadir} will become smaller while Δf_{QSS} is kept the same with the increase of virtual inertia constant.

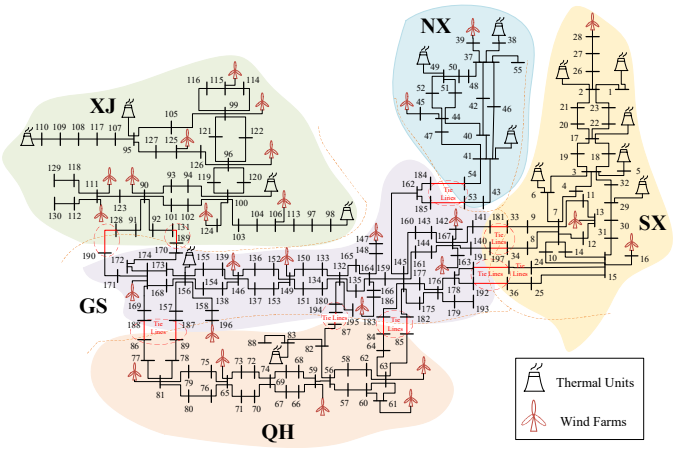

Fig.3. Topology of a provincial power system in China

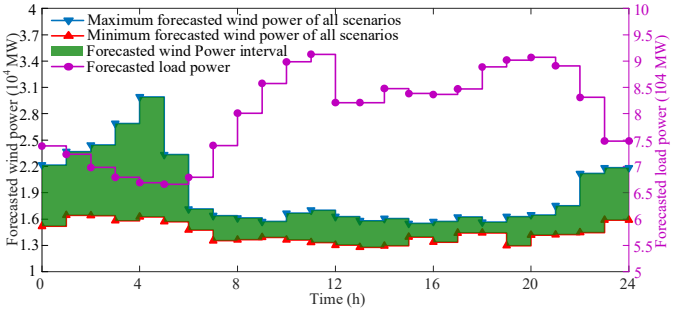

Fig. 4. Electric load and wind farm scenarios

Table II Comparisons with and without virtual inertia ($\Delta t^{\max} = 0.25\sum_{k\in\Omega_W} W_{k,s,t}$)

Metrics/Costs		Limits	Without λ	With λ		
				0.95	0.98	1.00
RoCoF		≤0.2	0.5518	0.2756	0.2334	0.1999
Δf_{Nadir}		≤0.5	0.7153	0.6024	0.5589	0.4969
Δf_{QSS}		≤0.2	0.3481	0.3481	0.3481	0.2000
C_{oper} (10^7)	SU/SD	--	1.838	2.718	2.718	3.218
	Gen.	--	15.17	15.19	15.19	15.17
C_{resev} (10^7)		--	1.119	1.119	1.119	1.122
C_{virt} (10^7)		--	0	0.600	1.300	2.100
C_{main} (10^8)		--	1.813	1.963	2.033	2.161

Table III Comparisons with different virtual inertia constant ($\Delta t^{\max} = 0.25\sum_{k\in\Omega_W} W_{k,s,t}$, λ=0.95)

Metrics/Costs		Limits	Hw_k=4s	Hw_k=6s	Hw_k=8s
RoCoF		≤0.2	0.2874	0.2756	0.2732
Δf_{Nadir}		≤0.5	0.6104	0.6024	0.6013
Δf_{QSS}		≤0.2	0.3481	0.3481	0.3481
C_{oper} (10^7)	SU/SD	--	2.967	2.718	1.869
	Gen.	--	15.19	15.19	15.18
C_{resev} (10^7)		--	1.119	1.119	1.119
C_{virt} (10^7)		--	0.600	0.600	0.750
C_{main} (10^8)		--	1.988	1.963	1.891

The UC solutions with (λ=0.95 and 1) and without frequency security are shown in Fig. 5, where more units will be committed as we increase of λ, allowing the system inertia to be increased. In particular, during peak load periods, more units will be needed to guarantee sufficient power reserves and system inertia to cope with possible wind power shortfalls.

The distribution of the system and virtual inertia for different disturbances $\Delta_t^{\max}$ is shown in Fig. 6. Here, increasing $\Delta_t^{\max}$ will lead to a larger system and virtual inertia. Moreover, during midnight hours (e.g., 1:00-5:00), the system load is low while the wind power penetration is high. Accordingly, less thermal generation will be needed at those hours and the system inertia contributed by thermal units will be low. Here, wind power variations are large and the system requires larger system inertia in order to guarantee the frequency security. The virtual inertia requirement is low during 8:00-22:00 due to the sufficient inertia is provided by thermal units.

The interval power flows on critical tie lines among the five provinces for 100 scenarios are shown in Fig. 7, where the power is transferred from Gansu to Ningxia, and from Qinghai to Gansu. Meanwhile, power flows are bi-directional on tie lines from Xinjiang to Gansu and Shaanxi to Gansu, which are determined by wind power generation variations.

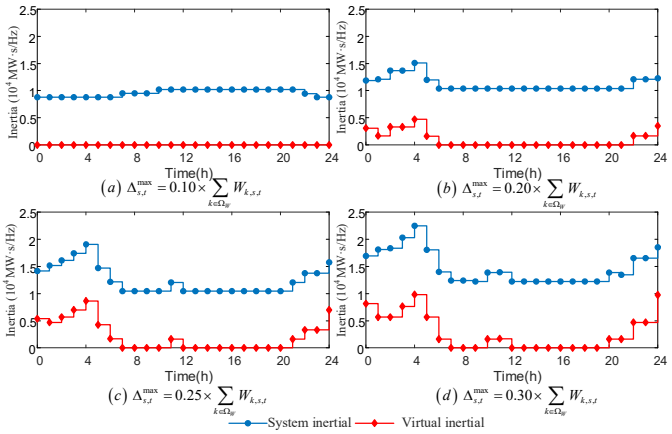

Fig. 6 Distribution of system and virtual inertia

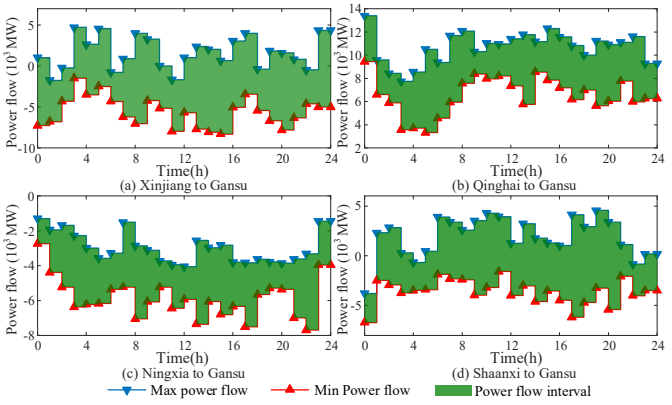

Fig. 7 Critical tie lines among provinces (λ=0.95)

Then, frequency comparisons with and without frequency security are shown in Fig. 8, where neglecting the frequency security constraints will lead to a 176% violation of RoCoF,

This article has been accepted for publication in a future issue of this journal, but has not been fully edited. Content may change prior to final publication. Citation information: DOI 10.1109/TPWRS.2021.3051523, IEEE Transactions on Power Systems

0.22 Hz violation of Nadir frequency and 0.15 Hz violation of QSS frequency. We fix the total inertia for λ=1 and then remove the virtual inertia provided by WSS. The frequency comparisons are shown in Fig. 9, which indicates that the frequency will significantly drop without considering the virtual inertia because the power system lacks enough inertia to cope with disturbances. Both Δf_{Nadir} and RoCoF will violate allowable limits while Δf_{QSS} remains the same.

Furthermore, the frequency curves for 100 scenarios are presented in Fig. 10 when the wind farm output suddenly decreases at period 5 (i.e. 4:00-5:00). Here, we only select three representable scenarios for illustration purposes. It can be observed from Fig. 4 that the wind farm output is large at period 5, so the sudden decrease of wind farm output will have a significant impact on the power system frequency security. At this moment, the RoCoF, Δf_{QSS}, and Δf_{Nadir} of scenarios 46 and 73 do not exceed the limits, while scenario 2 will violate the limits. This is because the chance constraint with λ=0.95 will allow the decision-maker to sacrifice the security of the system in order to decrease the total cost, where the probability of scenario 2 is very small.

Then, the scalability and the computation time are investigated in Table III for three methods including: directly using CPLEX, traditional Benders Decomposition (BD), and the proposed BBD. The computation time is increased by increasing the number of scenarios, i.e., K. However, CPLEX could only handle the small K case (e.g., $K\leq$50). We can reduce the number of constraints by neglecting the frequency constraints, which will lead to a shorter computation time. When λ=1, the computation time is relatively fast because BBD will be degenerated to a simple BD. When 0<λ<1, the computation times of both BD and BBD are longer because chance constraints introduce many binary variables. However, BBD requires fewer iterations (Iter.) than that of BD, so it runs faster than BD. Generally, the computation time can be improved by 10%-40% when the proposed BBD is applied. In addition, the results suggest that both BD and BBD can handle large K whereby the computation time is less than that of directly using CPLEX.

Finally, Table IV also compares the objective values of the three methods. The CPLEX is considered as the benchmark method. The objective values of both BD and BBD are nearly the same as that of CPLEX and the gap is smaller than 1%. This indicates that both methods, i.e., BD and BBD, can yield precise solutions. When 0<λ<1, the objective value of BD is slightly closer to that of CPLEX than that of BBD, suggesting that the BBD method is more precise. In addition, the results of BD and BBD are the same when λ=0 and λ=1, because BBD and BD are the same in the two cases.

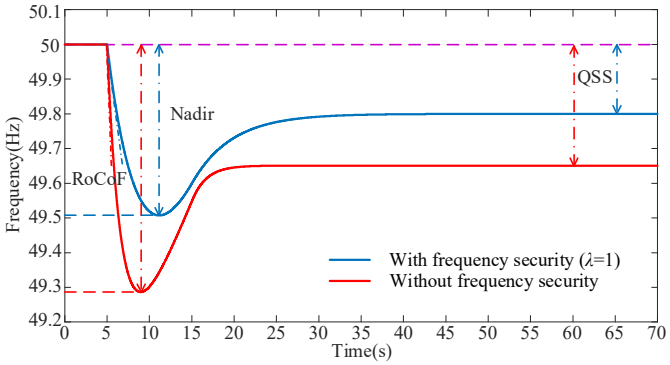

Fig. 8. Comparison of frequency with and without frequency security

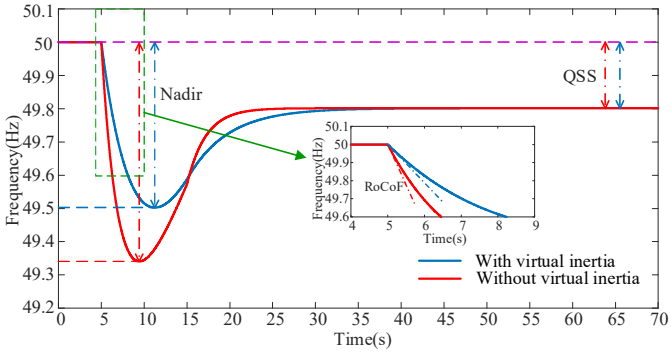

Fig. 9 Comparison of frequency with and without virtual inertia

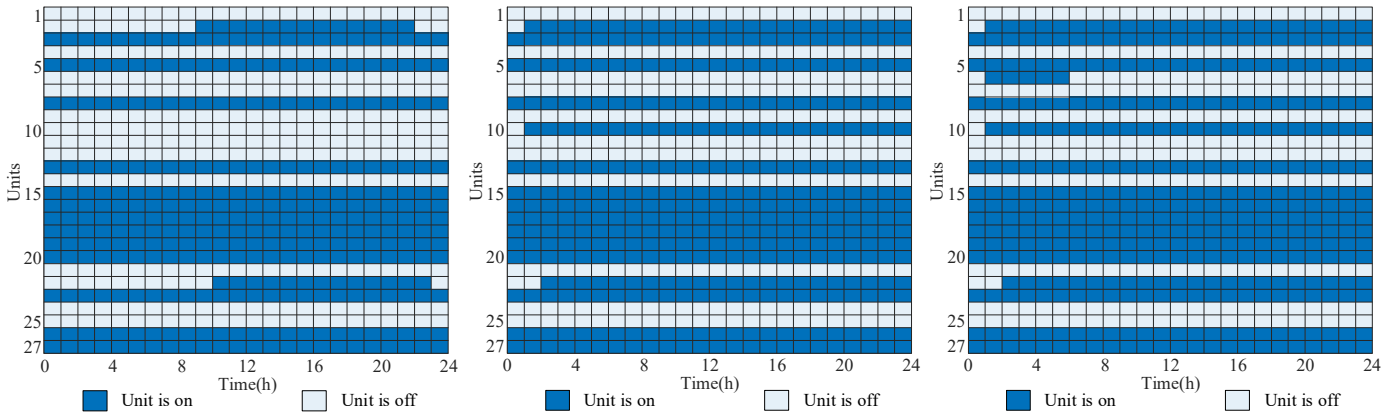

(a) without frequency security (b) with frequency security (λ=0.95) (c) with frequency security (λ=1)

Fig. 5 Comparisons of UC solutions with and without frequency security

Table IV Comparison of computation time and optimization results for the three methods

K	Λ	CPLEX			BD			BBD		
		Iter.	Time (s)	C_{main} (10^8)	Iter.	Time (s)	C_{main} (10^8)	Iter.	Time (s)	C_{main} (10^8)
10	without	--	672	1.829	4	118	1.819	4	118	1.819

	0.95		1561	1.985	8	389	1.975	6	312	1.979
	0.98		1687	2.044	9	441	2.034	7	362	2.036
	1.00		983	2.176	4	160	2.162	4	160	2.162
50	without		6892	1.844	7	786	1.830	7	786	1.830
	0.95		32864	2.005	16	2256	1.991	13	1949	1.997
	0.98		33456	2.068	15	2782	2.053	11	2100	2.057
	1.00		8324	2.197	7	965	2.193	7	965	2.193
100	without		--	--	5	1892	1.813	5	1892	1.813
	0.95		--	--	9	4435	1.963	8	3998	1.963
	0.98		--	--	11	5463	2.033	8	4011	2.033
	1.00		--	--	6	2567	2.161	6	2567	2.161

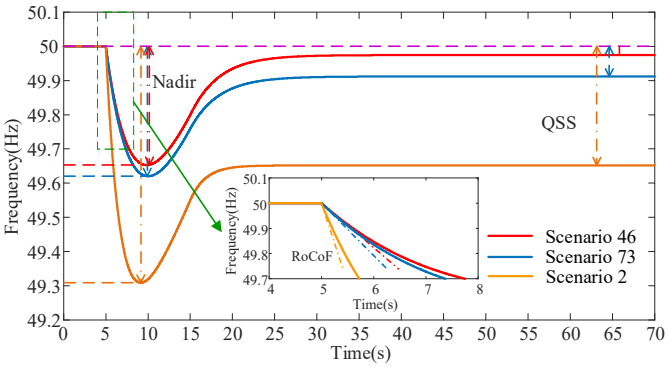

Fig. 10 Comparison of 100 scenarios with λ=0.95

V. CONCLUSION

This paper quantifies the frequency security and proposes TSCCSO to address the frequency security by optimally allocating the virtual inertia of WSS. To solve this model, an enhanced bilinear Benders decomposition method is proposed with strong valid cuts. The proposed enhanced bilinear Benders method can significantly improve the computational performance. Numerical results on a practical power system in China show that increasing the frequency security requirement will increase the ED cost in which case larger disturbances will also need higher virtual inertia to guarantee the frequency security. Future works will study the optimal planning and locations of WSS for the virtual inertia.

REFERENCES

[1] Y. Xu, T. Ding, M. Qu and P. Du, "Adaptive Dynamic Programming for Gas-Power Network Constrained Unit Commitment to Accommodate Renewable Energy With Combined-Cycle Units," *IEEE Trans. Sustain. Energy*, vol. 11, no. 3, pp. 2028-2039, July 2020.

[2] E. Du et al., "Operation of a high renewable penetrated power system with CSP plants: a look-ahead stochastic unit commitment model," *IEEE Trans. Power Syst*., vol. 34, no. 1, pp. 140-151, Jan. 2019.

[3] M. Shahidehpour, T. Ding, Q. Ming, C. Huang, Z. Wang and P. Du, "Multi-Period Active Distribution Network Planning Using Multi-Stage Stochastic Programming and Nested Decomposition by SDDIP," *IEEE Trans. Power Syst.*, in press. doi: 10.1109/TPWRS.2020.3032830.

[4] International Renewable Energy Agency: 'Renewable energy capacity statistics 2018', 2018. Available at http://www.irena.org, accessed 12 November 2018.

[5] J. Fang, H. Li, Y. Tang and F. Blaabjerg, "Distributed power system virtual inertia implemented by grid-connected power converters," *IEEE Trans. Power Electron.*, vol. 33, no. 10, pp. 8488-8499, Oct. 2018.

[6] J. F. Restrepo and F. Galiana, "Unit commitment with primary frequency regulation constraints," *IEEE Trans. Power Syst.*, vol. 20, no. 4, pp. 1588-1596, Nov. 2005.

[7] T. Inoue, H. Taniguchi, Y. Ikeguchi and K. Yoshida, "Estimation of power system inertia constant and capacity of spinning-reserve support generators using measured frequency transients," *IEEE Trans. Power Syst.*, vol. 12, no. 1, pp. 136-143, Feb. 1997.

[8] S. You, et al., "Non-invasive identification of inertia distribution change in high renewable systems using distribution level PMU," *IEEE Trans. Power Syst.*, vol. 33, no. 1, pp. 1110-1112, Jan. 2018.

[9] X. Cao, B. Stephen, I. F. Abdulhadi, C. D. Booth and G. M. Burt, "Switching markov gaussian models for dynamic power system inertia estimation," *IEEE Trans. Power Syst.*, vol. 31, no. 5, pp. 3394-3403, 2016.

[10] P. M. Anderson, "Power system control and stability," *IEEE Trans. Syst., Man, Cybern.. A, Syst., Humans,* vol. 15, no. 3, pp. 40-49, March 1995.

[11] M. Tavakoli, M. Power, L. Ruttledge, D. Flynn, "Load inertia estimation using white and grey-box estimators for power systems with high wind penetration," *Power Plants&Power Syst. Cont.*, vol. 8pp. 399-404, 2012.

[12] A. Mullane, G. Bryans, M. Malley, "Kinetic energy and frequency response comparison for renewable generation systems," *2015 International Conference on Future Power Systems,* Amsterdam, pp: 6-10, 2015.

[13] P. Daly, D. Flynn and N. Cunniffe, "Inertia considerations within unit commitment and economic dispatch for systems with high non-synchronous penetrations,"*2015 IEEE Eindhoven Power Tech*, Eindhoven, pp. 1-6, 2015.

[14] A. Muzhikyan, T. Mezher and A. M. Farid, "Power system enterprise control with inertial response procurement," *IEEE Trans. Power Syst.*, vol. 33, no. 4, pp. 3735-3744, July 2018.

[15] J. F. Restrepo and F. Galiana, "Unit commitment with primary frequency regulation constraints," *IEEE Trans. Power Syst.*, vol. 20, no. 4, pp. 1588-1596, Nov. 2005.

[16] T. Xu, W. Jang and T. Overbye, "Commitment of fast-responding storage devices to mimic inertia for the enhancement of primary frequency response," *IEEE Trans. Power Sys.,* vol. 33, no. 2, pp. 1219-1230, March 2018.

[17] Z. Zhang, E. Du, F. Teng, N. Zhang and C. Kang, "Modeling frequency dynamics in unit commitment with a high share of renewable energy," *IEEE Trans. Power Syst.*, in press. doi: 10.1109/TPWRS.2020.2996821.

[18] R. Doherty, G. Lalor, and M. O'Malley, "Frequency control in competitive electricity market dispatch," *IEEE Trans. Power Syst.*, vol. 20, no. 3, pp. 1588-1596, Aug. 2005.

[19] Y. Lee and R. Baldick, "A frequency-constrained stochastic economic dispatch model," *IEEE Trans. Power Syst.*, vol. 28, no. 3, pp. 2301-2312, 2013.

[20] F. Teng, V. Trovato and G. Strbac, "Stochastic scheduling with inertia-dependent fast frequency response requirements," *IEEE Trans. Power Syst.*, vol. 31, no. 2, pp. 1557-1566, March 2016.

[21] J. Ekanayake and N. Jenkins, "Comparison of the response of doubly fed and fixed-speed induction generator wind turbines to changes in network frequency," *IEEE Trans. Energy Convers.*, vol. 19, no. 4, pp. 800-802, Dec. 2004.

[22] Díaz-González, Francisco, et al. "Participation of wind power plants in system frequency control: Review of grid code requirements and control methods. "*Renew. Sust. Energy Rev.,* vol.34, pp: 551-564, 2014.

[23] P. Keung, P. Li, H. Banakar and B. T. Ooi, "Kinetic energy of wind-turbine generators for system frequency support," *IEEE Trans. Power Syst.*, vol. 24, no. 1, pp. 279-287, Feb. 2009.

[24] M. Kayikci and J. V. Milanovic, "Dynamic contribution of DFIG-based wind plants to system frequency disturbances," *IEEE Trans. Power Syst.,* vol. 24, no. 2, pp. 859-867, May 2009.

[25] P. Tielens and D. V. Hertem, "The relevance of inertia in power systems," *Renew. Sust. Energy Rev.*, vol. 55, pp. 999-1009, 2016.

[26] B. Rawn, M. Gibescu, W. Kling, "A static analysis method to determine the availability of kinetic energy from wind turbines," *2010 IEEE PES General Meeting*, 2010, pp: 1-8.

[27] G. Delille, B. Francois and G. Malarange, "Dynamic frequency control support by energy storage to reduce the impact of wind and solar

generation on isolated power system's inertia," *IEEE Trans. Sustain. Energy*, vol. 3, no. 4, pp. 931-939, Oct. 2012.
[28] W. J. Farmer and A. J. Rix, "Optimising power system frequency stability using virtual inertia from inverter-based renewable energy generation," *IET Renew. Power Gener.*, vol. 14, no. 15, pp. 2820-2829, Nov. 2020.
[29] M. H. Fini, M. E. H. Golshan, "Determining optimal virtual inertia and frequency control parameters to preserve the frequency stability in islanded microgrids with high penetration of renewables." *Electr. Power Syst. Res.,* vol.154, pp:13-22, Jan. 2018.
[30] B. K. Poolla, S. Bolognani and F. Dörfler, "Optimal placement of virtual inertia in power grids," *IEEE Trans. Autom. Control*, vol. 62, no. 12, pp. 6209-6220, Dec. 2017.
[31] L. Badesa, F. Teng and G. Strbac, "Simultaneous scheduling of multiple frequency services in stochastic unit commitment," *IEEE Trans. Power Syst.*, vol. 34, no. 5, pp. 3858-3868, Sept. 2019.
[32] A. F. Guillamóna, E. G. Lázarob, E. Muljadic, A. M. Garcíaa, "Power systems with high renewable energy sources: A review of inertia and frequency control strategies over time," *Renew. Sust. Energy Rev.*, vol. 115, pp. 109369- 109380. Nov. 2019.
[33] T. Ding, R. Bo, H. Sun, F. Li and Q. Guo, "A Robust Two-Level Coordinated Static Voltage Security Region for Centrally Integrated Wind Farms," *IEEE Trans. Smart Grid*, vol. 7, no. 1, pp. 460-470, Jan. 2016.
[34] T. Ding *et al*., "Duality-Free Decomposition Based Data-Driven Stochastic Security-Constrained Unit Commitment," *IEEE Trans. Sustain Energy*, vol. 10, no. 1, pp. 82-93, Jan. 2019.
[35] R. Lu, T. Ding, B. Qin, J. Ma, X. Fang and Z. Dong, "Multi-Stage Stochastic Programming to Joint Economic Dispatch for Energy and Reserve With Uncertain Renewable Energy," *IEEE Transa. Sustain. Energy*, vol. 11, no. 3, pp. 1140-1151, July 2020.
[36] B. Zeng, Y. An, and L. Kuznia, "Chance constrained mixed integer program: bilinear and linear formulations, and Benders decomposition," Optimization Online (http://www.optimization-online.org/DB_FILE/ 2014/ 03/4295.pdf), 2014.
[37] J. Morren, S. W. H. de Haan, W. L. Kling and J. A. Ferreira, "Wind turbines emulating inertia and supporting primary frequency control," *IEEE Trans. Power Syst.*, vol. 21, no. 1, pp. 433-434, Feb. 2006.
[38] P. Kundur, N. J. Balu NJ, Lauby MG. Power system stability and control vol. 7. New York: McGraw-hill; 1994.
[39] X. Liu and W. Xu, "Economic load dispatch constrained by wind power availability: a here-and-now approach," *IEEE Trans. Sustain. Energy*, vol. 1, no. 1, pp. 2-9, April 2010.
[40] Z. Shu and P. Jirutitijaroen, "Latin hypercube sampling techniques for power systems reliability analysis with renewable energy sources," *IEEE Trans. Power Syst.*, vol. 26, no. 4, pp. 2066-2073, Nov. 2011.
[41] T. Ding, Z. Zeng and M. Qu, https://github.com/QuDaming/100-Scenarios-of-the-Wind-Farm-Output/find/main, 2020.

Tao Ding (SM'19) received the B.S.E.E. and M.S.E.E. degrees from Southeast University, Nanjing, China, in 2009 and 2012, respectively, and the Ph.D. degree from Tsinghua University, Beijing, China, in 2015. During 2013 and 2014, he was a Visiting Scholar in the Department of Electrical Engineering and Computer Science, University of Tennessee, Knoxville, TN, USA. During 2019 and 2020, he was a Visiting Scholar of the Robert W. Galvin Center for Electricity Innovation at Illinois Institute of Technology. He is currently a Professor in the State Key Laboratory of Electrical Insulation and Power Equipment, the School of Electrical Engineering, Xi'an Jiaotong University. His current research interests include electricity markets, power system economics and optimization methods, and power system planning and reliability evaluation. Dr. Ding is an editor of IEEE Transactions on Power Systems, IEEE Power Engineering Letters, IET Generation Transmission & Distribution and CSEE JPES.

Ziyu Zeng (S'20) received the B.S. degree from the School of Electrical Engineering, Xi'an Jiaotong University, Xi'an, China, in 2018. He is currently working toward the M.S. degree at Xi'an Jiaotong University. His major research interests include power system optimization and renewable energy integration.

Ming Qu (S'19) received the B.S. degree from the School of Electrical Engineering, Shandong University, Jinan, China, in 2017. He is currently working toward the Ph.D. degree at Xi'an Jiaotong University. His major research interests include power system optimization and renewable energy integration.

João P. S. Catalão (Senior Member, IEEE) received the M.Sc. degree from the Instituto Superior Técnico (IST), Lisbon, Portugal, in 2003, and the Ph.D. degree and Habilitation for Full Professor ("Agregação") from the University of Beira Interior (UBI), Covilha, Portugal, in 2007 and 2013, respectively.

Currently, he is a Professor at the Faculty of Engineering of the University of Porto (FEUP), Porto, Portugal, and Research Coordinator at INESC TEC. He was also appointed as Visiting Professor by North China Electric Power University (NCEPU), Beijing, China. His research interests include power system operations and planning, distributed renewable generation, power system economics and electricity markets, demand response and smart grid.

Mohammad Shahidehpour (LF'01) received an Honorary Doctorate from the Polytechnic University of Bucharest, Romania, in 2009. He is the Bodine Chair Professor and Director of the Robert W. Galvin Center for Electricity Innovation at Illinois Institute of Technology. He is a Life Fellow of IEEE, Fellow of the American Association for the Advancement of Science (AAAS), Fellow of the National Academy of Inventors (NAI), Laureate of KIA (Khwarizmi International Award), and an elected member of the US National Academy of Engineering. He is listed as a highly cited researcher on the Web of Science (ranked in the top 1% by citations demonstrating significant influence among his peers).